A Worldwide Network of Radars for Space Domain Awareness in Low Earth Orbit

James Rowland
LeoLabs, Inc
Darren McKnight[1], Bonnie Prado Pino[1], Benedikt Reihs[2], Matthew A. Stevenson[1]
[1]*LeoLabs, Inc*
[2]*Independent*

ABSTRACT

We present LeoLabs' worldwide network of phased-array radars. LeoLabs' network consists of four operational radar sites, two Ultra High Frequency and two S-band, with an additional S-band radar site under construction. We show quantitative analyses of the radar network's performance, including network and component level performance metrics. Comparisons to independent data sets demonstrate the instrumentation's accuracy and precision, while comparisons amongst the radar sites demonstrate the self-consistency of LeoLabs' measurements and precision of LeoLabs' orbital state vector estimates. We also show simulated network performance in cataloging and tracking previously-uncataloged resident space objects. We show how the network can be used for a variety of tasks in addition to tracking RSOs in LEO. We provide characterization of the network's performance during Launch and Early Orbit phase operations. Finally, we show that LeoLabs' radars are capable of detecting objects in geostationary orbit (GEO). This proves that phased-array radars are a viable technology for tracking objects in GEO.

1. INTRODUCTION

LeoLabs' network of phased-array radars is designed to meet the tracking and monitoring needs of the rapidly growing commercial sector in low Earth orbit (LEO). Debris in the LEO environment poses a serious risk to assets when tracking and monitoring are unavailable. In addition to the immediate risk posed by existing orbital debris, there is future risk in the event that two massive derelict resident space objects (RSOs) collide [1]. Competent risk mitigation strategies must include multiple efforts: using best practices for operational satellites to prevent additional risk, removing large high-risk RSOs from orbit, and tracking and monitoring orbital debris to enable avoidance, when necessary.

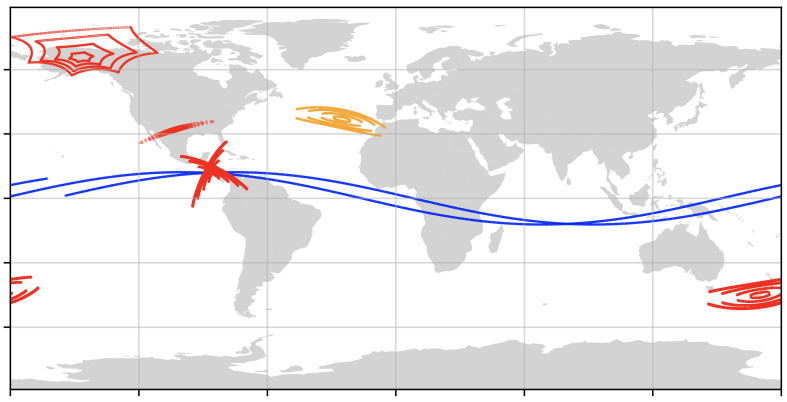

Fig. 1: Map of LeoLabs' radar network. Radar fields-of-view contours are plotted in red for operational sites, and orange for sites under construction. An equatorial orbit is plotted in blue highlighting the need for near equatorial radars like the Costa Rica Space Radar.

LeoLabs' radar network consists of two UHF radar sites, and two S-band radar sites designed to track sub-10 cm objects in LEO. A third S-band radar site is under construction, and LeoLabs' roadmap puts one radar on every continent (except Antarctica) by end of 2022. Data from all radar sites are collected and processed into higher level data products, including ephemerides, conjunction data messages (CDMs), and orbit change events. These are delivered via a web-based API (application programming interface) and platform at https://platform.leolabs.space.

The most recent addition to LeoLabs' network is the Cost Rica Space Radar (CRSR) commissioned on April 22nd, 2021 in Guanacaste, Costa Rica. The East facing trough is pictured in Fig. 2. CRSR has two unique features in LeoLabs' network. First, the site is nearly equatorial. This allows LeoLabs to track objects in low-inclination orbits for the first time. Second, the radars produces an "X"-shaped field-of-view (FOV). This FOV design is intentional, allowing CRSR to track RSOs in low inclination orbits with both fields of view, while also increasing the probability of observing high inclination orbits with at least one field of view.

Fig. 2: Photograph of the East trough of the Costa Rica Space Radar in Guanacaste, Costa Rica. This S-band radar has been operational since it was commissioned in April 2021.

The Azores Space Radar (AZSR) is currently under construction in the Azores archipelago on the island of Santa Maria, Portugal. The design of AZSR combines aspects of the previous two S-band radar sites in LeoLabs' radar network. AZSR has a parallel dual trough design shown in Fig. 3 that is reminiscent of the Kiwi Space Radar (KSR) dual trough design. However the trough shape and offset feed are taken from the design of CRSR. Radars commissioned prior to 2021 were discussed in a previous report [2], those are: Poker Flat Incoherent Scatter Radar (PFISR), Midland Space Radar (MSR), and KSR.

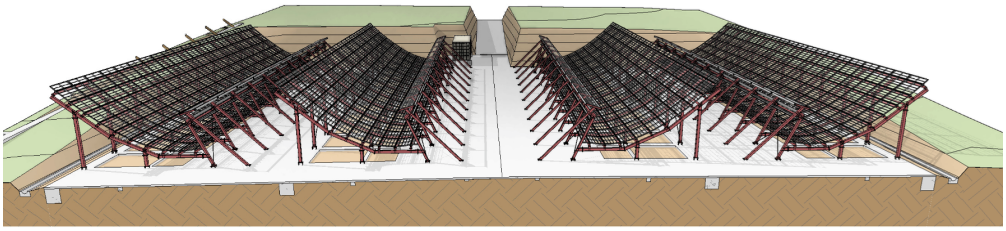

Fig. 3: Rendering of the Azores Space Radar currently under construction on Santa Maria Island, Portugal.

The capability of LeoLabs' radar network is determined by two synergistic factors. The first factor is the performance of individual radars in the network. The phased array design of LeoLabs' radars allows them to track multiple objects simultaneously. The radars are capable of tracking more than 1,000 objects per hour [2]. The second factor is the collective performance of the network as determined by the number of radars in the network and their placement around the globe. In Section 2 we characterize the performance of LeoLabs' radar network in term of these two

factors. In Section 3 we show simulated network performance in cataloging and tracking previously-uncataloged RSOs.

We highlight the flexibility of LeoLabs' radar network by showing how it can be used for a variety of tasks in addition to tracking RSOs in LEO. The network has proven effective for tracking deployments during the Launch and Early Orbit Phase (LEOP) of LEO missions. In Section 4 we provide characterization of the network's performance during LEOP operations, including examples from selected missions. In Section 5 we report on the detection of satellites in geostationary orbits made using the Costa Rica Space Radar. This is an impressive feat given the design constraints of LeoLabs' radars. This proves that phased-array radars are a viable technology for tracking objects in GEO.

2. PERFORMANCE CHARACTERISTICS

We study the performance of LeoLabs' radar network in terms of individual radar performance, and in terms of network level characteristics like revisit time and orbital coverage. The benefits that come with improving holistic performance metrics can be surprising. At the network level, building more radar sites decreases revisit times. This leads to a dramatic improvement in LeoLabs' data products. Orbit change detection is more sensitive. State vectors are more accurate due to shorter propagation times. Covariance estimates are smaller and more realistic. This ultimately leads to more frequent, more accurate, and more actionable CDMs.

In Fig. 4 we show the revisit statistics of LeoLabs' radar network with variable radar combinations. The data include LeoLabs measurements over a three-month period from 2021-05-01 to 2021-07-31. The measurement with the highest signal to noise ratio (SNR) from each radar pass is used for analysis. The revisit time for a radar pass is the time elapsed since the previous radar pass for the same target. With only two radars the tail is long and the most likely revisit time is one sidereal day. The median revisit time is 23.8 hours. Adding more radars suppresses the tail and dramatically increases the number of passes with revisit time less than 12 hours. The median revisit time with a four site network is only 8.4 hours. Revisit times will continue to decrease as more radars are built.

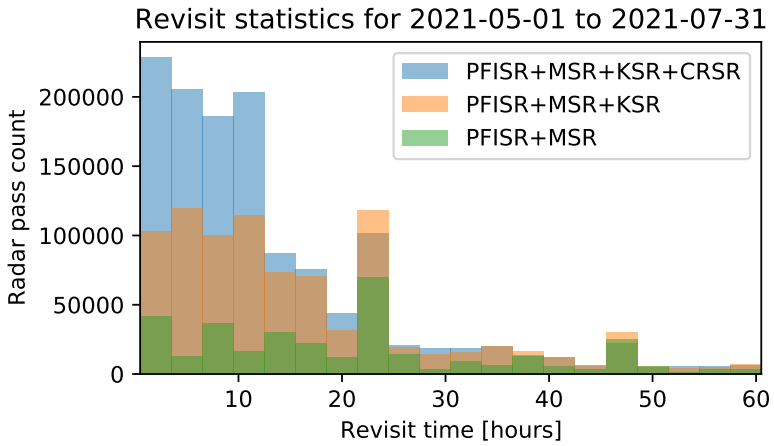

Fig. 4: Revisit time statistics with variable radar combinations. Increasing the number of radars in the network dramatically reduces revisit times, which leads to improvements in LeoLabs data products.

Adding radar sites to the network also increases orbit coverage if sites are chosen carefully. In Fig. 5 we show the count of unique objects observed by LeoLabs' network as a function of time with 30 day bins from 2020-07-01 to 2021-07-31. There is an overall upwards trend due to Starlink launches. In April LeoLabs commissioned the Costa Rica Space Radar which resulted in an increase in unique detections. CRSR has detected 498 objects from the public catalog that were previously undetected by the LeoLabs radar network. The placement of CRSR near the equator enables LeoLabs' network to detect the Hubble Space Telescope and other objects in low inclination orbits.

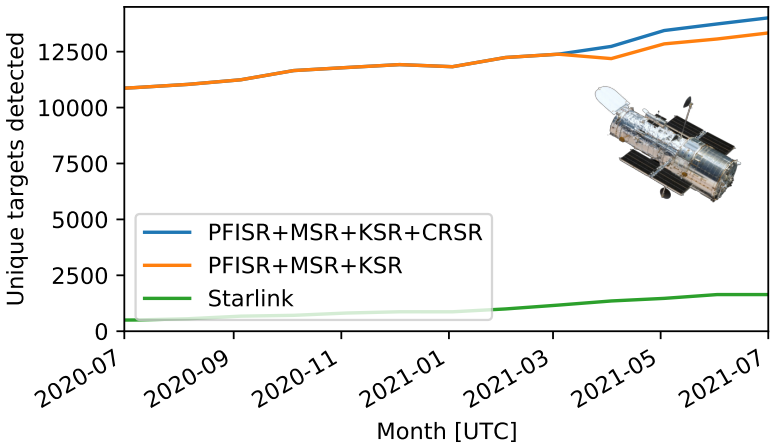

Fig. 5: Unique targets detected with variable radar combinations. The count of operational Starlink satellites is plotted to show that the upward trend in unique targets detected is caused by the rapid pace of Starlink launches. The Costa Rica Space Radar was commissioned on April 2021 leading to a noticeable increase in object counts. Newly detected objects include the Hubble Space Telescope pictured inset.

Moving now to the performance of individual radars in the network, we characterize the radars in terms of their measurement accuracy and precision. To determine measurement precision self-consistently we use LeoLabs state vectors as a source of truth. LeoLabs state vectors are made by filtering radar measurements. To avoid complications arising from correlations between measurements and state vectors, we choose state vectors that include radar measurements up to but not including the measurement under test. The state vector is used to predict range and doppler values, and these are then used to compute range and doppler residuals for the measurement under test. For range and doppler values sampled from normal distributions, and for state vectors sampled from a multi-normal distribution, the residual values are also normally distributed.

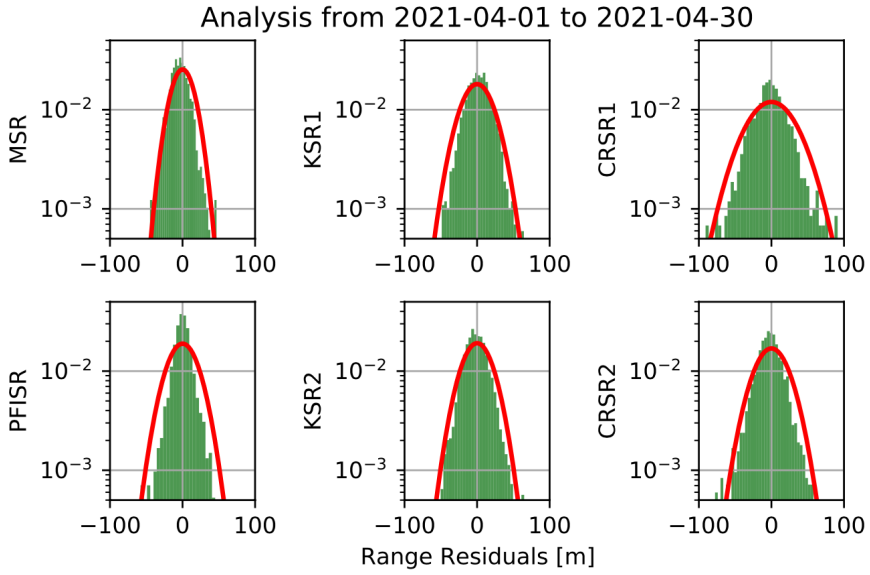

Fig. 6: Self-consistent measurement residuals computed using LeoLabs' state vectors as reference states. Fitted normal distributions are plotted as red curves on top of the empirical distributions shown as green histograms.

In Fig. 6 we plot the distribution of range residuals for measurements from different radars using LeoLabs' state

vectors as ground truth. Fitted normal distributions are plotted as red curves on top of the empirical distributions. Measurement precision is reported in Table 1; an identical analysis was performed for doppler measurements and the results are also included.

Next we use ephemerides from the International Laser Ranging System (ILRS) to determine the accuracy and precision of LeoLabs' measurements. Similar to the LeoLabs state vector based analysis, ILRS state vectors are used to predict reference range and doppler values. Range and doppler residuals are then computed from with respect to the predicted values. The covariances of ILRS state vectors are typically small enough that errors in the reference range and doppler values can be ignored relative to errors in LeoLabs' measurements [3]. Therefore the distribution of range residuals is normal with non-zero mean due to measurement bias, and standard deviation corresponding to the standard deviation of LeoLabs' range measurements. The same applies for the distribution of doppler residuals. Biases are removed from LeoLabs' measurements as part of the processing pipeline; they are reported here only to show the quality of raw measurements. We compute the bias and precision (reported as one standard deviation) of residuals in 3 day windows. The bias and precision values are then grouped into 30 day windows (10 values per window) to determine a 95% confidence interval. The bias and precision values are plotted in Fig. 7 for 2021-01-01 to 2021-07-01. The residuals are stable within a 95% confidence interval except for CRSR2 which had a 7 m shift in bias between June and July.

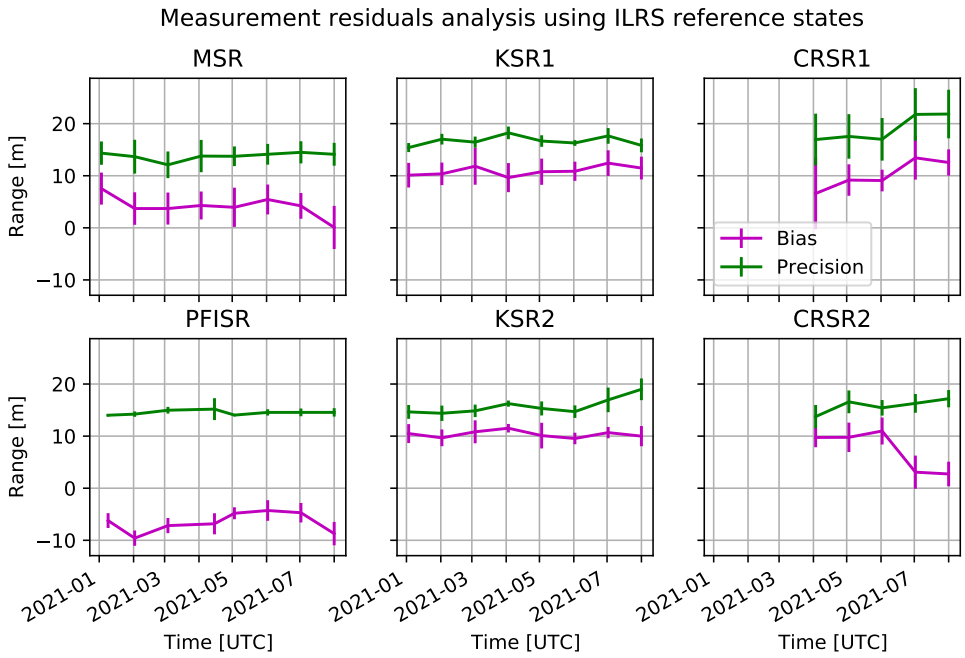

Fig. 7: Analysis of range residuals using ILRS state vectors for reference. The bias and precision are shown with 95% confidence intervals.

Results from the LeoLabs and ILRS state vector analyses are collected and summarized in Table 1. Also included in the table are theoretical estimates for range and doppler precision based on instrument design parameters. In addition to range and doppler measurements, LeoLabs' radars are also capable of measuring the angular position of targets. This is possible using correlator processing techniques that take advantage of the phased array design. Analysis of angular measurements is forthcoming.

Instrument	Range precision [m]			Doppler precision [cm/s]		
	Theory	Self-consistent	ILRS	Theory	Self-consistent	ILRS
CRSR1	20	19	19±14	15	45	15±6
CRSR2	20	15	16±5	15	52	17±7
KSR1	20	15	17±4	15	51	16±6
KSR2	20	14	16±5	15	45	17±6
MSR	20	13	14±7	30	62	25±8
PFISR	15	12	14±2	350	116	400±300

Table 1: Precision of LeoLabs' measurements from three sources: theoretical estimates, self-consistent estimates made using propagated state vectors from the LeoLabs API, and external estimates made using state vectors from ILRS ephemerides. ILRS precision estimates are reported with 95% confidence intervals.

3. SEARCH COMPLETENESS SIMULATION

Search radars in LeoLabs' network use a 2-trough design. To discover a previously uncataloged object the object must pass through the fields-of-view of both troughs during the same pass. The detection of uncataloged targets happens through a serendipitous discovery process, i.e., it happens by chance during tracking of targets already in the catalog. Following object discovery an initial orbit determination (IOD) is performed using measurements from both troughs. This orbit is used to schedule followup observations at additional radar sites.

In Fig. 8 we show an example of object discovery made using LeoLabs' serendipitous search detection system. The range, time, intensity (RTI) plots show the processed signal data used to make detections. The corresponding doppler, time, intensity is also shown; we will refer to these plots together as RTI plots. Detections from the RTI data are plotted as a scatter. Detections are grouped into tracklets labeled "Coherent Tracklets." A tracklet is a collection of detections that have range and doppler values consistent with a polynomial fit in time, i.e., the detections follow a trajectory consistent with physics. The intended target is distinguished by its position relative to the predicted position plotted as a transparent gray curve with the scatter points. The serendipitously detected target is at 1180 km range and -3200 m/s doppler.

The accompanying polar plot in Fig. 8 illustrates the scheduling process for the second FOV. A circular orbit fit is performed using data from the first FOV. The orbit fit is doubly degenerate, so there are two blue curves labeled "1st instrument." Detection made at the second FOV is plotted as an orange point. This is consistent with the fitted orbit from the discovered target, i.e., the detection is overlapping the fitted orbit. As a sanity check, the second FOV detection is used to fit a circular orbit (orange curve) to confirm that the observations are consistent with detections made in the first FOV (blue point).

We use a search completeness simulation to model the entire search process, including serendipitous discovery, IOD, and subsequent observation at other radar sites in the network. The goal is to understand the effect of site selection on the search process, and the dependence of completeness on orbital parameters, not to predict catalog size per se. The simulation includes effects due to probability of detection modeled by considering the range of the target, the IOD covariance, the shape of radar beams, and the radar cross section (RCS) of the target. For the simulation we use a RCS corresponding to a 10 cm diameter sphere. Simulation results are reported in terms of completeness percentage as a function of time and orbital elements (excluding mean anomaly). Given an initial population of objects uniformly distributed in mean anomaly, the completeness percentage for that orbit represents the fraction of those objects that are catalogued at or before the specified time.

We note that the simulation provides a lower bound on completeness for several reasons. First, the simulation uses a 100 km range window for searching. This is currently correct for KSR and CRSR, but for these sites, AZSR, and future S-band sites there is an improved processing architecture that permits a 2000 km range window. Increasing the range window leads to an corresponding increase in discovery rate of roughly 20x compared to what is reported in the simulation. Second, the simulation models a serendipitous discovery process for existing RSOs. Completeness values will be higher if orbits with larger populations are given dedicated search time. Lastly, the rate of discovery is underestimated for breakup events. During a breakup event a debris cloud is generated. The positions of objects in the cloud are correlated with the position of the originating RSO. Compared to existing RSOs, these would be cataloged more rapidly even when using serendipitous search.

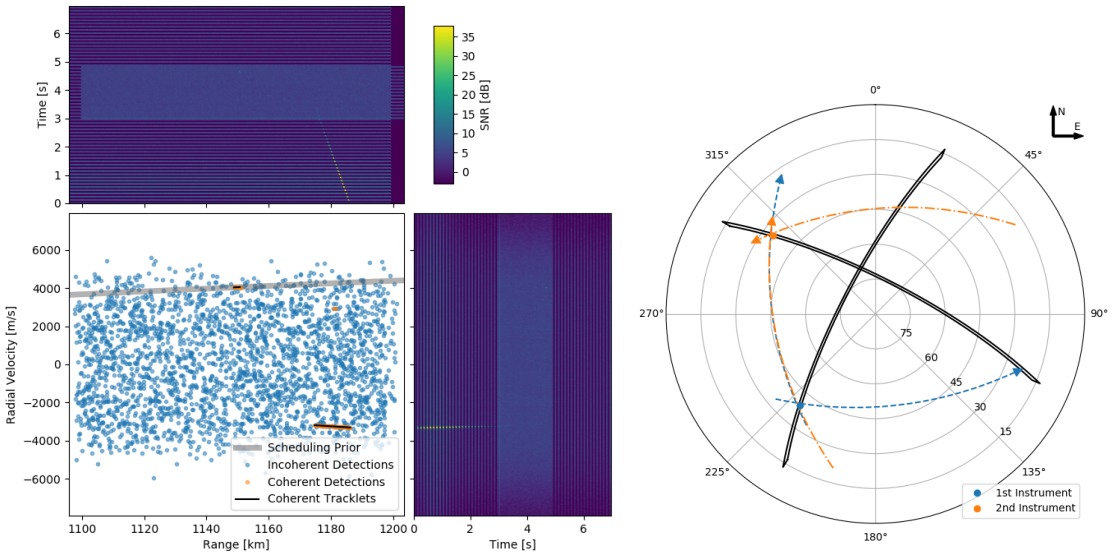

Fig. 8: Example detection from LeoLabs' serendipitous discovery system. Two targets are detected and labeled as "Coherent Tracklets" in the scatter plot. The intended target is close to the predicted trajectory indicated by a transparent black curve. The other target is used to schedule a followup experiment at the second FOV. The circular orbit fits from the first instrument, labeled "1st instrument", is used to schedule the second FOV. Detections are made in the second FOV, and the correspond circular orbit fit is labeled "2nd intsrument."

Analysis of simulation results is stratified by considering different combinations of future radar sites. In Fig. 9 we show how completeness depends on network size for RSOs with 702 km altitude and 33 degrees inclination to illustrate site selection effects in an extreme case. Unspecified sites are labeled as Future Site 1-3 (FS1-FS3). The low inclination of the orbit means that sites far from the equator, such as KSR, cannot observe the orbit. Adding the equatorial site FS1 to the network dramatically increases catalog completeness. Additional sites are not equatorial so completeness depends entirely on the performance of CRSR and FS1. In Fig. 9 we also show completeness results for an orbit with a moderate inclination of 54 degrees. All radars in the network participate in cataloging and tracking objects in this orbit. Site FS3 contributes more to completeness than site FS2. Catalog completeness increases with each radar added to the network, eventually tapering off as completeness approaches 100%.

In Fig. 10 we show the evolution of completeness as a function of time for a radar network with six S-band radar sites. The chosen orbit has an altitude of 800 km and inclination of 98.9 degrees. The population of untracked debris in this orbit should be large due to the intentional break-up of the Fengyun-1C spacecraft on 11 January 2007 [4]. Cataloging via serendipitous search is an example of a coupon collector problem; thus, the rate of discovery (derivative of completeness) is nearly constant for small times, and asymptotically approaches zero as completeness approaches 100%. At the end of the two-year simulation period, the completeness value is 40%. This corresponds to an average discovery rate of 0.4% per week. Upgrades to LeoLabs' radar processing architecture will increase this rate by up to 20x. If the breakup event had occurred during the cataloging period, the correlation between debris positions and the position of Fengyun-1C would have increased the discovery rate significantly.

In Fig. 9 and Fig. 10 we report completeness as a percentage of objects observed in a particular orbit, not as a percentage of all untracked RSOs. A completeness of 10% for one particular orbit does not imply that only 10% of objects in LEO are cataloged. Orbits with higher populations must be scaled by the corresponding RSO population to get the object count. Completeness over all orbits is then an average over individual orbit completeness percentages weighted by the fraction of untracked RSOs in those orbits. In Fig. 11 we use the population of cataloged objects to represent a hypothetical distribution of untracked RSOs, and we report completeness in terms of the number of objects observed as a function of altitude and inclination. Low completeness for low inclination values is expected with only two equatorial sites in the network, and because of the small population of RSOs at those inclinations. The number of objects observed near 800km altitude and 96 degrees inclination is high due to the large population of cataloged RSOs in those orbits.

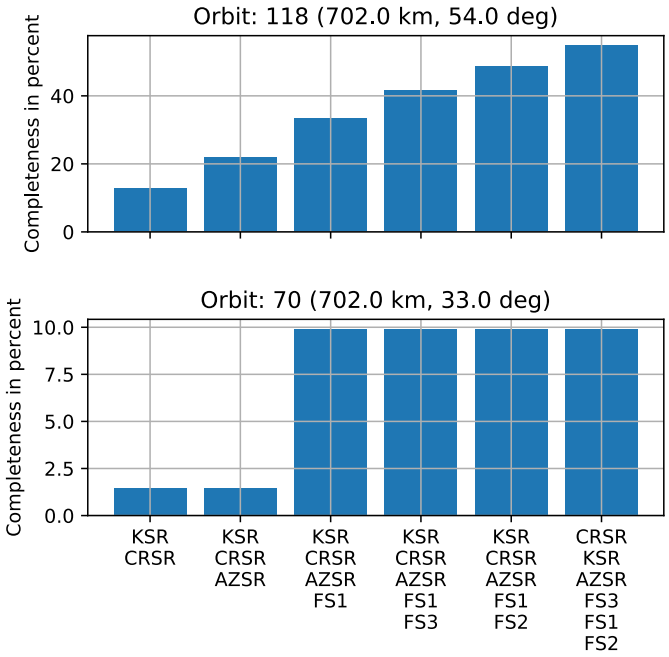

Fig. 9: Two year search completeness simulation results for different orbits as a function of variable radar site selection. For Orbit 70 the inclination is low and only CRSR and Future Site 1 (FS1) are able to contribute to completeness. For Orbit 118 the inclination is higher and radars in the network contribute, so the final completeness value is higher. The low completeness for Orbit 70 does not have a significant impact on overall catalog completeness since the population of untracked RSOs at 33 deg is small.

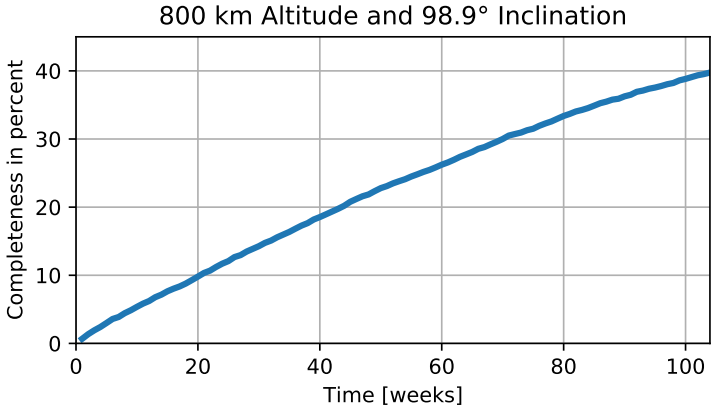

Fig. 10: Evolution of search completeness as a function of time for a radar network with six radar sites. The completeness value applies to the population of RSOs in an orbit with 800 km altitude and 98.9 degrees inclination, corresponding to the location of debris from the intentional breakup of Fengyun-1C. These completeness values are a lower bound; they do not include effects from future improvements in LeoLabs' processing architecture, or correlations between object positions after a breakup event.

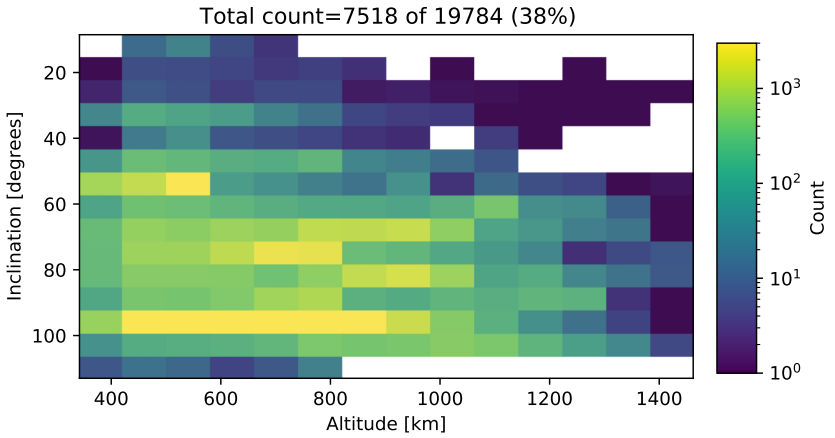

Fig. 11: Completeness counts for a hypothetical untracked RSO population sampled from the public catalog. The final completeness value over all orbits in the simulation is 38% after two years with a six radar site network. Completeness at 96 degrees inclination is high because of the large population of RSOs and because of the layout of LeoLabs' radar network. This can be improved with targeted search applied to orbits with high populations of untracked RSOs.

4. LAUNCH AND RE-ENTRY TRACKING

The need for support during the Launch and Early Orbit Phase (LEOP) of operations is growing. Operators sometimes spend days or weeks trying to establish communications after deployment. In the worst case, satellites do not survive LEOP operations, and contact is never established. LeoLabs offers tracking and monitoring services starting at deployment and continuing until objects are able to be cataloged. To understand the effectiveness of LeoLabs' radar network for LEOP operations we study data from 10 Starlink deployments in 2021. These 10 deployments are highly consistent in two regards. First, all deployments have 60 Starlink satellites and 4 tension rods that must be tracked. Second, the insertion state vector in an Earth-fixed frame is similar in every mission. This consistency leads to nearly identical radar pass geometries which allows us to study target observability as a statistical property.

Fig. 12 shows observation statistics from the 10 Starlink deployments. The data is grouped into two hour bins during the first 4 days after launch. In each bin we compute the percentage of the 64 targets that were observed for each deployment. We further group the data based on whether the percentage of targets observed is greater than 0%, between 50% and 90%, or greater than 90%. The resulting stratified histogram illustrates the frequency and tracking completeness of detections made.

The distribution is peaked due to the consistency of deployment state vectors (in an Earth-fixed frame) between launches. For long times any variability between deployments is exaggerated, which leads to a broadening of the distribution. The observation frequency is typically high, with a majority of missions observing targets multiple times per day. Maximum observability occurs during a window between 40 and 42 hours after launch. During the first 12 hours after launch the separation between deployments is typically smaller than the resolution of LeoLabs' radars which precludes the observation of all targets. The radar pass within the first two hours after launch is never able to resolve more than 50% of targets. After the first 24 hours missed targets are caused by poor pass geometry. As we continue to increase the size of LeoLabs' radar network we will see a concomitant increase in observation frequency and quality.

LeoLabs' radar network is also capable of tracking non-cooperative launches. As a demonstration of this capability we present a case study. In May 2021 we tracked the uncontrolled re-entry of a Long March 5B rocket body. We made 8 observations of the target from 2021-05-05 03:30 UTC to 2021-05-08 11:20 UTC. The last observation was made at MSR less than 13 hours before the rocket body crashed at approximately 2021-05-09 02:30 UTC. Measurements from a CRSR radar pass are shown in Fig. 13. The figure shows range and doppler measurements as scatter points along with the TLE used to schedule the radars. Even with poor prior data, LeoLabs' radars are capable of observing targets due to the large range and doppler processing window used.

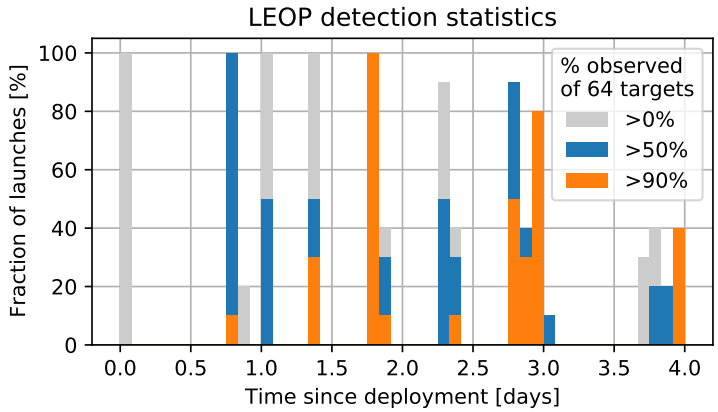

Fig. 12: Detection statistics for LeoLabs' Launch and Early Orbit service. Statistics are from 10 Starlink deployments in 2021. The stratified histogram represents the distribution of radar passes as a function of time for which the give fraction of targets were observed. Maximum observability occurs between 40 and 42 hours.

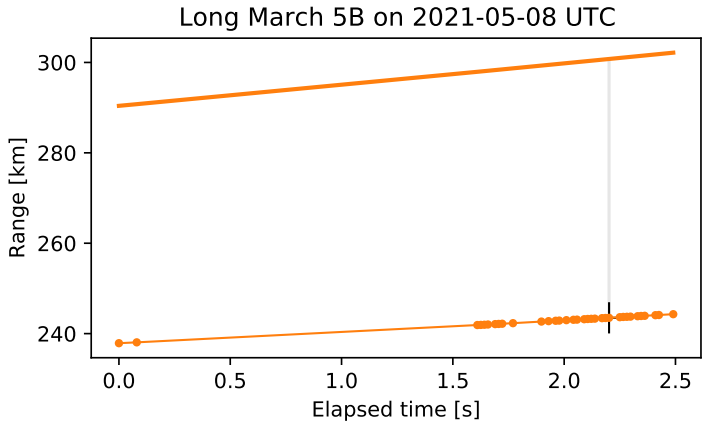

Fig. 13: Scatter plot of radar measurements from a rocket body on re-entry. The prior state used to schedule the radar is shown as a solid curve. Even with limited prior data LeoLabs' radar network is capable of observing targets.

5. GEOSTATIONARY ORBIT DETECTIONS

As a final demonstration of the capabilities of the LeoLabs radar network, we show that it is possible to detect objects in geostationary orbit using a phased array radar. We chose two targets based on size and observability: the Geostationary Operational Environmental Satellite GOES-14, and the non-operational communications satellite AsiaSat 2 (later renamed to AMOS-5i). These satellites have low inclination orbits that pass through the FOV of CRSR, and both targets are large, with orbital masses of approximately 1,500 kg each [5, 6].

Fig. 14 shows detections of AsiaSat 2 made using CRSR. We scheduled CRSR to gaze at the predicted position of AsiaSat 2 for more than 20 minutes. The data was processed using one minute coherent integrations. The peak detection for AsiaSat 2 had a SNR of more than 30 dB. The target was in the FOV for less than 10 minutes. The detections are confirmed by plotting the range and doppler values as scatter points alongside the range and doppler values predicted using a TLE plotted as a black curve.

To observe GOES-14 we scheduled CRSR to gaze at the satellite's orbit for more than one hour. For GOES-14 we used one minute coherent integrations and achieved radar detections with a SNR of more than 10 dB. Unlike AsiaSat

2, GOES-14 stayed in the radar FOV throughout the entire observation period which allowed us to capture a longer track of the target.

To the best of our knowledge, these are the first detections of geostationary RSOs made by a commercially owned and operated phased array radar. We note that LeoLabs' radars are designed first and foremost to track objects in LEO. Some of the design decisions made to optimize for LEO tracking introduce limitations for GEO tracking. The one-dimensional FOV and the power budget of LeoLabs' radars make GEO tracking challenging. In spite of these limitations LeoLabs' radars are capable of detecting objects in GEO. Phased-array radars designed specifically for GEO tracking would offer performance exceeding that of CRSR. These results prove that phased-array radars are a viable technology for tracking objects in GEO.

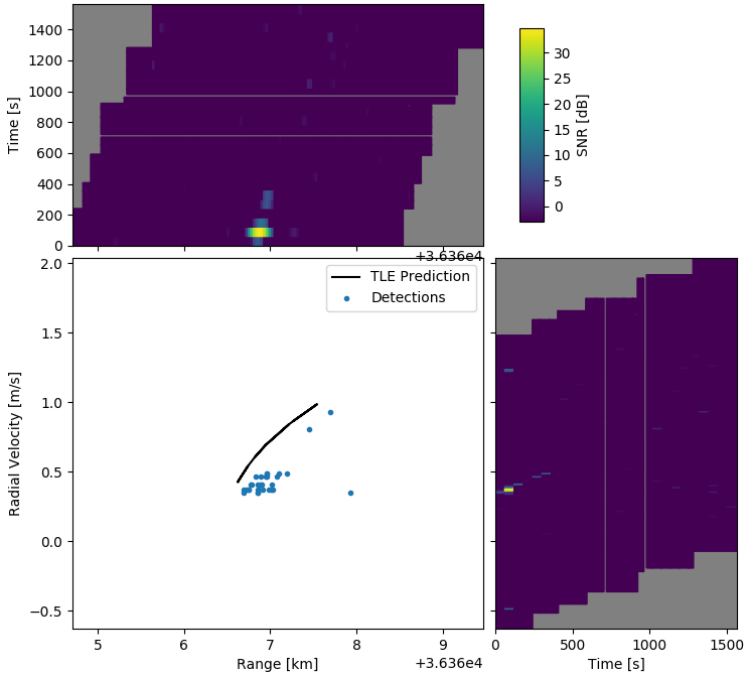

Fig. 14: RTI plot of the detection of AsiaSat 2 made using the Costa Rica Space Radar. The false-color plots indicate signal power in different time, range, and doppler bins. The detection is significant enough that the target is visible by eye in the RTI plot. Individual detections are shown as a scatter plot along with the predicted state of the target.

6. CONCLUSIONS

At its foundation LeoLabs set out to solve a problem. Orbital debris poses a serious risk to assets in low Earth orbit. That risk is driven by untracked debris already in orbit, and by possible future collisions between massive derelict resident space objects. LeoLabs provides a solution for risk mitigation in the form of a web-based platform and API powered by data from its worldwide network of phased array radars.

LeoLabs' S-band radars are capable of tracking sub-10 cm RSOs with 15 m range precision and 15 cm/s doppler precision. The phased-array design of LeoLabs' radars allows for tracking objects on different orbits simultaneously. Going beyond individual radar capabilities, LeoLabs' radars are uniquely capable as a network. In its present state the network allows for coverage of all orbits with a median revisit time of 8.4 hours. These metrics will continue to improve as the network grows, and a concomitant improvement in data products is expected. This will ultimately lead to more frequent, more accurate, and more actionable CDMs. Simulation results show the impact of site selection and orbit variation on catalog completeness. LeoLabs' radar sites are chosen to prioritize detection in high risk orbits. The serendipitous discovery process used in the simulation provides a worst case estimate for completeness; completeness increases with targeted search, or after a breakup event when debris positions are correlated. AZSR and future S-band sites will have a 2000 km range window for searching which increases discovery rate by roughly 20x.

In addition to meeting LeoLabs' design goals of tracking and monitoring orbital debris in LEO, LeoLabs' radar network has proven itself capable for a wide range of space domain awareness tasks. LeoLabs' network provides tracking and monitoring during the launch and early orbit phase of operations, with multiple observed passes per day, and >90% of targets observed within the first 48 hours after launch. LEOP detection statistics will improve as the network expands. LeoLabs' radar network is also capable of tracking objects undergoing uncontrolled re-entry.

Finally, we have shown that LeoLabs' S-band phased array radars are capable of detecting objects in geostationary orbit. This is an impressive feat given the design constraints of LeoLabs' radars. Nevertheless the radars make strong detections with a signal to noise ratio greater than 30dB. This proves that phased-array radars are a viable technology for GEO space surveillance.

REFERENCES

[1] Darren McKnight, Matthew Stevenson, Chris Kunstadter, and Rohit Arora. Updating The Massive Collision Monitoring Activity-creating A Leo Collision Risk Continuum. In *European Conference on Space Debris*, Darmstadt, Germany, April 2021.

[2] Matthew A Stevenson, Michael Nicolls, Inkwan Park, and Chris Rosner. Measurement Precision and Orbit Tracking Performance of the Kiwi Space Radar. In *Advanced Maui Optical and Space Surveillance (AMOS) Technologies Conference*, Maui, Hawaii, September 2020.

[3] David A Vallado, James Woodburn, and Tom Johnson. Sequential Processing of ILRS Observations – Experiences over the last 5 years. In *International Workshop on Laser Ranging*, November 2018.

[4] Nicholas L. Johnson, E. Stansbery, J.-C. Liou, M. Horstman, C. Stokely, and D. Whitlock. The characteristics and consequences of the break-up of the Fengyun-1C spacecraft. *Acta Astronautica*, 63(1-4):128–135, July 2008.

[5] Donald H. Martin. *Communication satellites*. AIAA, 2000.

[6] Boeing. GOES N Data Book. Technical Report CDRL PM-1-1-03, National Aeronautics and Space Administration Goddard Space Flight Center, February 2005.